Skyrme forces and the fusion-fission dynamics of the ^{132}Sn + ^{64}Ni → ^{196}Pt* reaction

Deepika Jain, Raj Kumar, and Manoj K. Sharma
School of Physics and Materials Science, Thapar University, Patiala 147004, India

Raj K. Gupta
Department of Physics, Panjab University, Chandigarh 160014, India

(Received 18 November 2011; revised manuscript received 24 January 2012; published 22 February 2012)

The dependence of the fusion-fission process on Skyrme forces is studied by using the dynamical cluster-decay model (DCM) and the ℓ-summed extended-Wong model in the ^{132}Sn + ^{64}Ni → ^{196}Pt* reaction, where the nuclear proximity potential is obtained by using the semiclassical extended Thomas-Fermi (ETF) approach in the Skyrme energy density formalism (SEDF) under the frozen density approximation. The DCM gives an excellent fit to the measured fusion evaporation residue (ER) and the fission cross sections below and above barrier energies, with ER data needing "barrier lowering" at below-barrier energies for each Skyrme force (an in-built property of the DCM). The fission cross sections show a contribution of quasifission (qf) at the above-barrier two or three highest energies, depending on the Skyrme force. Calculations are illustrated for three Skyrme forces, GSkI, SSk, and SIII. Another interesting result is that there is a change of fission mass distribution from a predominantly asymmetric one to a symmetric one with a decrease in the N/Z ratio of the compound nucleus, independent of the choice of nuclear interaction potential, which gives an opportunity to address the isospin effects in the Pt* nucleus. Within the ℓ-summed extended-Wong model we find that the GSkI and SSk forces fit the total fusion cross-section data exactly, whereas the SIII force needs "barrier modification" in order to fit the data at below-barrier energies. This happens because the isospin and neutron-proton asymmetry nature of GSkI and SSk forces is different from that of the SIII force, and because the center-of-mass energy $E_{\mathrm{c.m.}}$ dependence of the barrier height for the SIII force and that of Blocki *et al.* [Ann. Phys. (NY) **105**, 427 (1977)] differs strongly (by a constant amount of ∼7 MeV) from those for GSKI and SSk forces. Note that, because of the associated preformation factor with each fragment, the DCM has the advantage of treating various decay processes separately, whereas the Wong model describes only the total fusion cross section, a sum of cross sections due to all contributing processes.

DOI: 10.1103/PhysRevC.85.024615 PACS number(s): 25.70.Jj, 24.10.−i, 25.60.Pj, 27.80.+w

I. INTRODUCTION

A compound nucleus, depending on its mass, disintegrates by emitting multiple light particles (the evaporation residues, or ER), followed by fission (fusion-fission), and the noncompound quasifission (qf) or deep inelastic collision (DIC) process of a dinuclear system, where projectile- and target-like fragments are seen in the decay channel. Thus, for a compound nucleus reaction, the fusion cross section is defined as the sum of the fusion-evaporation cross section σ_{ER}, the fission cross section σ_{fiss}, and the quasifission cross section σ_{qf}. Recently, an experiment was performed to produce the neutron-rich compound nucleus ^{196}Pt* by bombarding a radioactive ^{132}Sn beam on ^{64}Ni, and the σ_{ER} and σ_{fiss} were measured [1]. Interestingly, *at sub-barrier energies*, only the ER cross section is measured since fission of ^{196}Pt* is then not observed. On the other hand, at above-barrier energies, the qf component in the fission cross sections could not be separated because of the inverse kinematics of the ^{132}Sn + ^{64}Ni reaction, and because of the beam intensity being several orders of magnitude lower than that of the stable ^{112,118,124}Sn beams. In view of the known unexpected behavior of the fusion evaporation cross sections at energies far below the Coulomb barrier, i.e., the fusion hindrance seen in the coupled-channel calculations (ccc) [2,3] for some other Ni-induced reactions (^{58,64}Ni + ^{58,64}Ni and ^{64}Ni + ^{100}Mo), the experimental data on ^{132}Sn + ^{64}Ni reaction [1] offer an interesting opportunity to study the fusion and fusion-fission dynamics with different theoretical models. Here, in the following, we carry out such a study by using the dynamical cluster-decay model (DCM) of preformed clusters [4–8] and the ℓ-summed extended-Wong model [9,10] of Gupta and collaborators. Further importance of this work is that it involves a neutron-rich radioactive beam, and the nuclear structure effects of the incoming nuclei and/or decay products are shown to influence the fusion cross sections at near- and below-barrier energies.

Recently, the dynamical cluster-decay model (DCM) was applied [5] to study the decay of compound nuclear systems ^{176,182,188,196}Pt* formed in ^{64}Ni + ^{112,118,124}Sn and ^{132}Sn + ^{64}Ni reactions. A nice fitting of the data to ER and fission cross sections was obtained, except that the fission cross section σ_{fiss} showed some contribution of the quasifission (qf) process at the highest one or two energies. Besides qf, an in-built "barrier modification" effect was shown to be the essential requirement for fitting the data to both ER and fission at *below-barrier* energies, just as for other well known ^{64}Ni + ^{64}Ni and ^{64}Ni + ^{100}Mo reactions [6–8]. Another important result of this study was a change of the mass distributions from predominantly symmetric to asymmetric in going from light mass ^{176,182}Pt* to heavy mass ^{188,196}Pt* compound nuclei, which was found to be due to the deformations and orientations of fission fragments. Note that, in the work [5] based on the DCM, the pocket formula due to Blocki *et al.* [11] was used

for calculating the nuclear proximity potential. In the present study, we introduce the use of different Skyrme forces in DCM via the nuclear proximity potential obtained [12] from the semiclassical extended Thomas-Fermi (ETF) approach in the Skyrme energy density formalism (SEDF) [13–15] under the frozen density approximation [16]. Compared to the nuclear proximity potential due to Blocki *et al*., with fixed barrier height, position, and curvature, the nuclear proximity potential derived from the SEDF has the advantage of allowing the use of different Skyrme forces, having different barrier characteristics, to introduce the barrier modification effect for the best fit to data via different Skyrme forces. In other words, Skyrme forces provide the flexibility for a better comparison of data, since a large number of them are available that fit different ground-state properties of nuclei from different mass regions.

More recently, the above-mentioned nuclear proximity potential [12], derived from the SEDF-based ETF approach, has also been used [10] in the ℓ-summed extended-Wong model [9], at above as well as below barrier energies, for studying the ER and capture cross section of Ni- and Ca-induced reactions, respectively. The ℓ-summed extended-Wong model [9] is an extended version of the Wong formula [17], where the angular momentum effects are explicitly included and are found to contain the barrier modification effects due to ℓ-dependent barriers. Barrier modification or no barrier modification at sub-barrier energies in the ℓ-summed extended-Wong model is shown to depend not only on the choice of Skyrme force but also on the type of reaction under investigation. The $\sigma_{\rm ER}$ of the considered Ni-based reactions (^{58,64}Ni + ^{5864}Ni and ^{64}Ni + ^{100}Mo) at sub-barrier energies required different Skyrme forces for the best fit to data. It is of interest here to study the chosen ^{132}Sn + ^{64}Ni $\rightarrow$ ^{196}Pt* reaction also on the basis of the ℓ-summed extended-Wong model [9] using the Skyrme-force-based nuclear proximity potential [12].

In this paper, we show that the application of the DCM to the ^{132}Sn + ^{64}Ni reaction using three Skyrme forces, namely SIII, GSkI, and SSk, leads to a result similar to the one obtained using the nuclear potential of Blocki *et al*., for this as well as other ^{64}Ni + ^{112,118,124}Sn reactions [5]; i.e., nice fits to both ER and fission cross sections are obtained. The effect of using different Skyrme forces on "barrier lowering" at sub-barrier energies in ER data is studied. Besides this, the qf contribution in fission data is predicted at higher center-of-mass energies $E_{\rm c.m.}$, which increase with the decrease in barrier height due to different Skyrme forces. Furthermore, the extended Wong model is applied to the ^{132}Sn + ^{64}Ni reaction, showing different nature of fits for different Skyrme forces, i.e., just as for other Ni-based reactions (^{58,64}Ni + ^{58,64}Ni and ^{64}Ni + ^{100}Mo) [10], whereas the GSkI and SSk forces fit the data without any barrier adjustment, the force SIII needs barrier adjustment for the best fit at below-barrier energies.

The result of the previous paragraph raises the question of why some Skyrme forces are better than others, and better than an interaction like that of Blocki *et al*. Since stronger isospin effects are needed for tackling the steep fall of the cross sections at below Coulomb barrier energies [18], the recent parametrizations GSkI and SSk provide the appropriate isospin effects, whereas the older SIII parametrization and the potential of Blocki *et al*. are less sensitive toward neutron-proton asymmetry and isospin effects. Also, the old Skyrme force parametrization SIII differs from the very recent GSkI and SSk forces in that they contain the tensor coupling with the spin and the gradient terms. In addition, the GSkI force also includes three density-dependent interactions, discussed in the next section.

The paper is organized as follows: The formalism, in terms of both the DCM and extended Wong model using nuclear proximity potential derived from the SEDF-based ETF approach, is given in Sec. II. Nuclei are considered to be in the same plane, and deformations are included up to hexadecapole deformations (β_2–β_4) with optimum orientations $\theta^{\rm opt.}$ [19] in the DCM, but the orientations θ are integrated in the extended Wong model [10]. Note that $\theta^{\rm opt.}$ are only use for quadrupole deformations ($\beta_4 = 0$). Our calculations and results are presented in Sec. III, and a brief summary is given in Sec. IV.

II. THE FORMALISM

A. Skyrme energy density formalism in the semiclassical extended Thomas-Fermi approach

The energy density formalism defines the nuclear interaction potential as

$$V_N(R) = E(R) - E(\infty), \tag{1}$$

i.e., the nucleus-nucleus interaction potential as a function of separation distance, $V_N(R)$, is the difference of the energy expectation values E of the colliding nuclei that are overlapping (at a finite separation distance R) and those that are completely separated (at $R = \infty$), where

$$E = \int H(\vec{r})d\vec{r}, \tag{2}$$

with the Skyrme Hamiltonian density defined as [20]

$$\begin{aligned} H(\rho,\tau,\vec{J}) &= \frac{\hbar^2}{2m}\tau + \frac{1}{2}t_0\left[\left(1+\frac{1}{2}x_0\right)\rho^2 - \left(x_0+\frac{1}{2}\right)\left(\rho_n^2+\rho_p^2\right)\right] \\ &+ \frac{1}{2}\sum_{i=1}^{3} t_{3i}\rho^{\alpha_i}\left[\left(1+\frac{1}{2}x_{3i}\right)\rho^2 - \left(x_{3i}+\frac{1}{2}\right)\left(\rho_n^2+\rho_p^2\right)\right] \\ &+ \frac{1}{4}\left[t_1\left(1+\frac{1}{2}x_1\right) + t_2\left(1+\frac{1}{2}x_2\right)\right]\rho\tau \\ &- \frac{1}{4}\left[t_1\left(x_1+\frac{1}{2}\right) - t_2\left(x_2+\frac{1}{2}\right)\right](\rho_n\tau_n+\rho_p\tau_p) \\ &+ \frac{1}{16}\left[3t_1\left(1+\frac{1}{2}x_1\right) - t_2\left(1+\frac{1}{2}x_2\right)\right](\vec{\nabla}\rho)^2 \\ &- \frac{1}{16}\left[3t_1\left(x_1+\frac{1}{2}\right) + t_2\left(x_2+\frac{1}{2}\right)\right][(\vec{\nabla}\rho_n)^2+(\vec{\nabla}\rho_p)^2] \\ &- \frac{1}{2}W_0[\rho\vec{\nabla}\cdot\vec{J} + \rho_n\vec{\nabla}\cdot\vec{J}_n + \rho_p\vec{\nabla}\cdot\vec{J}_p] \\ &- A\left[\frac{1}{16}(t_1x_1+t_2x_2)\vec{J}^2 - \frac{1}{16}(t_1-t_2)\left(\vec{J}_p^2+\vec{J}_n^2\right)\right]. \end{aligned} \tag{3}$$

Here, $\rho = \rho_n + \rho_p$, $\tau = \tau_n + \tau_p$, and $\vec{J} = \vec{J}_n + \vec{J}_p$ are the nuclear, kinetic energy, and spin-orbit densities, respectively. m is the nucleon mass, and x_j, t_j $(j = 0, 1, 2)$, x_{3i}, t_{3i}, α_i, $(i = 1, 2, 3)$, W_0, and A are the Skyrme force parameters, fitted recently by Agrawal *et al.* [20], denoted GSkI, GSkII, and SSk forces. These authors modified the earlier well known [14,21] Hamiltonian density by introducing six additional parameters in the third term [two each of x_{3i}, t_{3i}, and α_i $(i = 1, 2)$], and an additional last term with constant $A = 1$ to account for tensor coupling with spin and gradient. For the other earlier fitted Skyrme forces [14,21], such as SIII, SV, SkM*, etc., the constants A, x_{3i}, t_{3i}, and α_i $(i = 2, 3)$, are all zero, and $t_{31} = \frac{1}{6}t_3$, $x_{31} = x_3$, and $\alpha_1 = \alpha$. It is important to note here that the parameters of the new forces GSkI, GSkII, and SSk were determined by fitting several properties of some normal and isospin-rich nuclei [20], and our present study deals with asymmetric and isospin-rich colliding nuclei where such forces are expected to give more realistic results. Since the barrier characteristics of the GSkII force lie in between the GSkI and SSk forces, we are using here only the GSkI and SSk forces in our calculations.

The kinetic energy density in the ETF method, considered here up to second-order terms, those being enough for numerical convergence [15], is ($q = n$ or p)

$$\begin{aligned}\tau_q(\vec{r}) = {} & \frac{3}{5}(3\pi^2)^{2/3}\rho_q^{5/3} + \frac{1}{36}\frac{(\vec{\nabla}\rho_q)^2}{\rho_q} + \frac{1}{3}\Delta\rho_q \\ & + \frac{1}{6}\frac{\vec{\nabla}\rho_q\cdot\vec{\nabla}f_q + \rho_q\Delta f_q}{f_q} - \frac{1}{12}\rho_q\left(\frac{\vec{\nabla}f_q}{f_q}\right)^2 \\ & + \frac{1}{2}\rho_q\left(\frac{2m}{\hbar^2}\right)^2\left(\frac{W_0}{2}\frac{\vec{\nabla}(\rho+\rho_q)}{f_q}\right)^2, \end{aligned} \tag{4}$$

with f_q as the effective-mass form factor,

$$\begin{aligned} f_q(\vec{r}) = {} & 1 + \frac{2m}{\hbar^2}\frac{1}{4}\left\{t_1\left(1+\frac{x_1}{2}\right) + t_2\left(1+\frac{x_2}{2}\right)\right\}\rho(\vec{r}) \\ & - \frac{2m}{\hbar^2}\frac{1}{4}\left\{t_1\left(x_1+\frac{1}{2}\right) - t_2\left(x_2+\frac{1}{2}\right)\right\}\rho_q(\vec{r}). \end{aligned} \tag{5}$$

Note that both τ_q and f_q are each functions of ρ_q and/or ρ only.

The spin $\vec{J}$ is a purely quantal property, and hence has no contribution in the lowest Thomas-Fermi (TF) order. However, at the ETF level, the second-order contribution gives

$$\vec{J}_q(\vec{r}) = -\frac{2m}{\hbar^2}\frac{1}{2}W_0\frac{1}{f_q}\rho_q\vec{\nabla}(\rho+\rho_q), \tag{6}$$

also a function of ρ_q and/or ρ alone.

For the frozen density approximation used here, the densities for the composite system are [16]

$$\begin{aligned} \rho &= \rho_1 + \rho_2, \\ \tau(\rho) &= \tau_1(\rho_1) + \tau_2(\rho_2), \\ \vec{J}(\rho) &= \vec{J}_1(\rho_1) + \vec{J}_2(\rho_2), \end{aligned} \tag{7}$$

with $\rho_i = \rho_{in} + \rho_{ip}$, $\tau_i(\rho_i) = \tau_{in}(\rho_{in}) + \tau_{ip}(\rho_{ip})$, and $\vec{J}_i(\rho_i) = \vec{J}_{in}(\rho_{in}) + \vec{J}_{ip}(\rho_{ip})$.

For the nuclear proximity potential, following Blocki *et al.* [11] and Gupta *et al.* [12,22,23], we introduce the slab approximation of semi-infinite nuclear matter with surfaces parallel to the x-y plane, moving in the z direction, and separated by distance s having minimum value s_0. Then, the interaction potential $V_N(R)$ between two nuclei separated by $R = R_1 + R_2 + s$, is given by

$$\begin{aligned} V_N(R) &= 2\pi\bar{R}\int_{s_0}^{\infty} e(s)ds \\ &= 2\pi\bar{R}\int\{H(\rho,\tau,\vec{J}) \\ &\quad - [H_1(\rho_1,\tau_1,\vec{J}_1) + H_2(\rho_2,\tau_2,\vec{J}_2)]\}dZ \\ &= 4\pi\bar{R}\gamma b\phi(D) = V_P(R) + V_J(R), \end{aligned} \tag{8}$$

where $V_P(R)$ and $V_J(R)$ are the spin-density independent and spin-density dependent parts of the nuclear interaction potential. $\bar{R} = R_1R_2/(R_1 + R_2)$ is the mean curvature radius, defining the geometry of the system, and $\phi(D)$ is the universal function in terms of a dimensionless variable $D = s/b$, with b as the surface width, defined later in Eq. (14). The nuclear surface energy constant $\gamma = 0.9517[1 - 1.7826(\frac{N-Z}{A})^2]$ MeV fm^{-2}. For further details on $\phi(D)$, etc., see Ref. [12].

For the nuclear density ρ_i of each nucleus, the T-dependent, two-parameter Fermi density (FD) distribution for the slab approximation is given by [12]

$$\begin{aligned} \rho_i(z_i) &= \rho_{0i}(T)\left[1 + \exp\left(\frac{z_i - R_i(T)}{a_i(T)}\right)\right]^{-1}, \\ -\infty &\leqslant z \leqslant \infty, \end{aligned} \tag{9}$$

with $z_2 = R - z_1 = [R_1(\alpha_1, T) + R_2(\alpha_2, T) + s] - z_1$, central density

$$\rho_{0i}(T) = \frac{3A_i}{4\pi R_i^3(T)}\left[1 + \frac{\pi^2 a_i^2(T)}{R_i^2(T)}\right]^{-1}, \tag{10}$$

and the radii for spherically symmetric deformed nuclei

$$R_i(\alpha_i, T) = R_{0i}(T)\left[1 + \sum_{\lambda}\beta_{\lambda i}Y_{\lambda}^{(0)}(\alpha_i)\right]. \tag{11}$$

The spherical or half-density nuclear radius R_{0i} and surface thickness parameters a_i at $T = 0$ are obtained by fitting the experimental data [24,25] to respective polynomials in the nuclear mass region $A = 4$–238 [12], as

$$\begin{aligned} R_{0i}(T=0) &= 0.9543 + 0.0994A_i - 9.8851\times10^{-4}A_i^2 \\ &\quad + 4.8399\times10^{-6}A_i^3 - 8.4366\times10^{-9}A_i^4 \\ a_i(T=0) &= 0.3719 + 0.0086A_i - 1.1898\times10^{-4}A_i^2 \\ &\quad + 6.1678\times10^{-7}A_i^3 - 1.0721\times10^{-9}A_i^4. \end{aligned} \tag{12}$$

In Eq. (11), $\lambda = 2, 3, 4, \ldots$ are the multipole deformations, and α_i are the angles between radius vector $R_i(\alpha_i)$ and the symmetry axis, measured clockwise from the symmetry axis. For the estimation of s_0, we refer to [26] for coplanar nuclei.

The T dependence in the above formulas are then introduced as in Ref. [27],

$$R_{0i}(T) = R_{0i}(T=0)[1+0.0005T^2],$$
$$a_i(T) = a_i(T=0)[1+0.01T^2]. \quad (13)$$

Also, the surface width b is made T dependent [28],

$$b(T) = 0.99(1+0.009T^2), \quad (14)$$

where T is related to the incoming center-of-mass energy $E_{\rm c.m.}$ or the compound nucleus (CN) excitation energy $E^*_{\rm CN}$ via the entrance channel Q_{in} value, as

$$E^*_{\rm CN} = E_{\rm c.m.} + Q_{in} = \frac{1}{a}A_{\rm CN}T^2 - T \quad (T \text{ in MeV}), \quad (15)$$

with $a = 9$ or 10, respectively, for intermediate-mass or superheavy systems. $Q_{in} = B_1 + B_2 - B_{\rm CN}$, with binding energies B taken from [29]. Furthermore, since $\rho_i = \rho_{n_i} + \rho_{p_i}$, for nucleon density we define

$$\rho_{n_i} = (N_i/A_i)\rho_i \quad \text{and} \quad \rho_{p_i} = (Z_i/A_i)\rho_i. \quad (16)$$

B. The dynamical cluster-decay model (DCM)

The DCM is worked out in terms of the collective coordinates of mass (and charge) asymmetry $\eta = (A_1 - A_2)/(A_1 + A_2)$ [and $\eta_Z = (Z_1 - Z_2)/(Z_1 + Z_2)$], relative separation R, the multipole deformations $\beta_{\lambda i}$, and the orientations θ_i ($i = 1, 2$) of two nuclei in the same plane. In the DCM, we define the compound nucleus (CN) decay cross section in terms of partial wave analysis as

$$\sigma = \sum_{\ell=0}^{\ell_{\rm max}} \sigma_\ell = \frac{\pi}{k^2}\sum_{\ell=0}^{\ell_{\rm max}}(2\ell+1)P_0^\ell P_\ell, \quad k = \sqrt{\frac{2\mu E_{\rm c.m.}}{\hbar^2}}, \quad (17)$$

where the preformation probability P_0^ℓ refers to η motion and the penetrability P_ℓ to R motion. $\ell_{\rm max}$ is the maximum angular momentum, fixed here for the light-particle cross section approaching zero, i.e., $\sigma_{\rm ER}(\ell) \to 0$ at $\ell = \ell_{\rm max}$.

P_0 for each ℓ is the solution of the stationary Schrödinger equation in η, at a fixed R,

$$\left[-\frac{\hbar^2}{2\sqrt{B_{\eta\eta}}}\frac{\partial}{\partial\eta}\frac{1}{\sqrt{B_{\eta\eta}}}\frac{\partial}{\partial\eta} + V(\eta)\right]\psi^\nu(\eta) = E^\nu_\eta\psi^\nu(\eta), \quad (18)$$

and the penetrability P_ℓ is the WKB integral

$$P_\ell = \exp\left[-\frac{2}{\hbar}\int_{R_a}^{R_b}\{2\mu[V(R) - Q_{\rm eff}]\}^{1/2}dR\right], \quad (19)$$

with $V(R_a, T) = V(R_b, T) = TKE(T) = Q_{\rm eff}$ for the two turning points. $Q_{\rm eff}$ is the effective Q value of the decay process, and the first turning point $R_a = R_1(\alpha_1, T) + R_2(\alpha_2, T) + \Delta R(\eta, T)$.

Then, the deformation- and orientation-dependent fragmentation potential in Eq. (18), at any temperature T, is given by

$$V(\eta, T) = \sum_{i=1}^{2} V_{\rm LDM}(A_i, Z_i, T) + \sum_{i=1}^{2}\delta U\exp\left(-\frac{T^2}{T_0^2}\right) + V_C(R, Z_i, \beta_{\lambda i}, \theta_i, T) + V_N(R, A_i, \beta_{\lambda i}, \theta_i, T) + V_\ell(R, A_i, \beta_{\lambda i}, \theta_i, T). \quad (20)$$

Here, $V_{\rm LDM}$ from Ref. [30] and δU from Ref. [31] are the T-dependent liquid drop and shell correction energies. V_C and V_ℓ are the T-dependent Coulomb and angular-momentum-dependent potentials, respectively. V_N is the nuclear proximity potential discussed in Sec. II A using the ETF approach of SEDF under the frozen density approximation.

$\Delta R(T)$, in the definition of R_a above, is the neck-length parameter, assimilating the neck formation effects [32,33]. The choice of ΔR for a best fit to the data allows us to define the effective barrier lowering parameter $\Delta V_B(\ell)$ for each ℓ as the difference between the actually used barrier $V(R_a, \ell)$ and the top of the calculated barrier $V_B(\ell)$,

$$\Delta V_B(\ell) = V(R_a, \ell) - V_B(\ell). \quad (21)$$

Note, since ΔV_B is defined as a negative quantity, the actually used barrier is effectively lowered. It is relevant to point out here that, since the empirically fitted neck length $\Delta R(T)$ is unique, the barrier lowering parameter $\Delta V_B(E_{\rm c.m.})$ is also a uniquely fixed quantity.

C. The ℓ-summed extended-Wong model

According to Wong [17] the fusion cross section in terms of partial waves, for two deformed and oriented nuclei lying in same plane, is also given by Eq. (17), but with $P_0^\ell = 1$ for each ℓ, i.e., there is no preformation factor, and hence the model is not applicable to various observed decay processes. Thus, the extended ℓ-summed Wong model is a special case of the DCM with $P_0^\ell = 1$ and penetrability P_ℓ calculated in the Hill-Wheeler [34] approximation of an inverted harmonic oscillator for the total interaction potential $V(R)$ of the incoming channel, whereas the same in the DCM is calculated by the WKB integral for each decay channel. In the Hill-Wheeler approximation, the penetrability P_ℓ, in terms of the barrier height V_B^ℓ and curvature $\hbar\omega_\ell$, is given by

$$P_\ell = \left[1 + \exp\left(\frac{2\pi\left(V_B^\ell - E_{\rm c.m.}\right)}{\hbar\omega_\ell}\right)\right]^{-1}, \quad (22)$$

with $\hbar\omega_\ell$ evaluated at the barrier position $R = R_B^\ell$ corresponding to barrier height V_B^ℓ. It is important to realize here that in the present analysis only the barrier height V_B^ℓ, position R_B^ℓ, and curvature $\hbar\omega_\ell$ of $V(R)$ come in to play, the depth of pocket playing no role.

Carrying out the ℓ summation empirically for a best fit to the measured total cross section, as described by Gupta and collaborators [9], and upon integrating over the angles θ_i, we get the fusion cross section $\sigma_{\rm fus}$ as a function of $E_{\rm c.m.}$.

III. CALCULATIONS AND RESULTS

We have made our calculations for the fusion-evaporation residues and fusion-fission of the ^{196}Pt* compound nucleus using the DCM, and for the total fusion cross section using the ℓ-summed extended-Wong model, with nuclear proximity potential obtained from the SEDF-based ETF method for three illustrative Skyrme forces GSkI, SSk, and SIII, and compared with the potential of Blocki *et al.* [5]. These forces cover a large range of the barrier characteristics (V_B, R_B, and $\hbar\omega$). The effects of orientations and deformations are included, as mentioned in the Introduction.

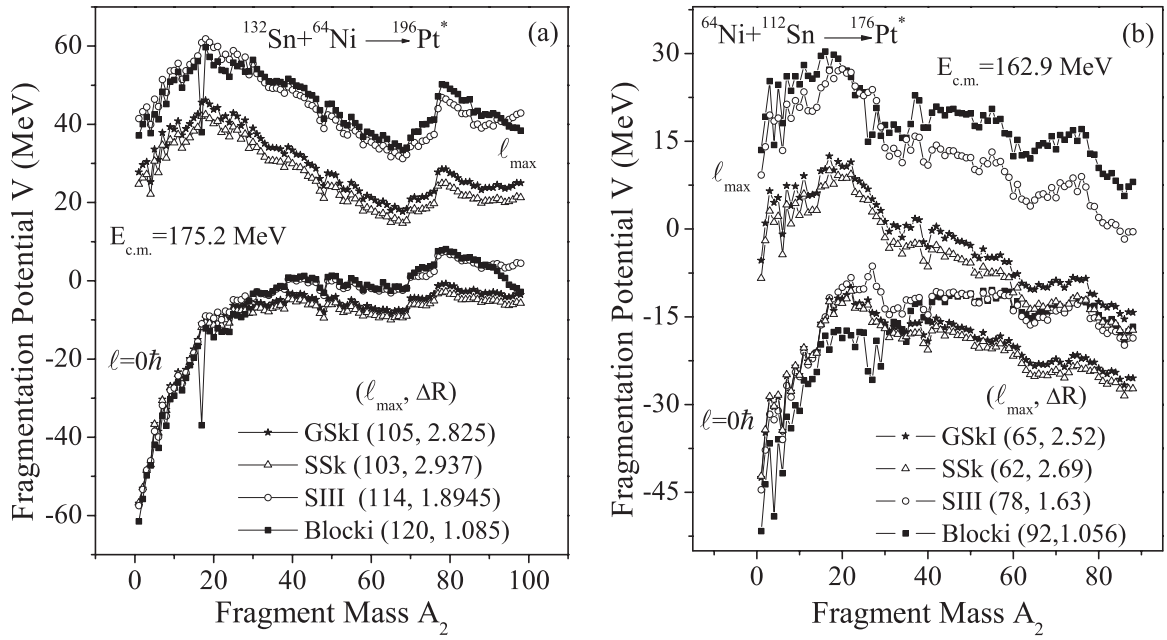

FIG. 1. (a) Fragmentation potential $V(A_2)$ for the decay of compound nucleus ^{196}Pt*, plotted at $\ell = 0$ and ℓ_{max} values, using different Skyrme forces and compared with interaction of Blocki *et al*. from Ref. [5]. (b) The same as (a) but for the compound nucleus ^{176}Pt*.

A. Decay of ^{196}Pt* using the DCM

First of all we look at the fragmentation potentials $V(A_2)$ for the three Skyrme forces, compared with the potential due to Blocki *et al*., plotted in Fig. 1(a) for the $\ell = 0$ and ℓ_{max} cases. We notice that the forces GSkI (solid line with star) and SSk (solid line with hollow triangle) behave nearly alike, since, for both the forces, the same fragments contribute to the decay processes. Also ℓ_{max} values are close to each other (see columns 3 and 4 in Table I), and the potential energy minima are stronger at the asymmetric fragments than the symmetric

TABLE I. The ER and fission cross sections for the ^{196}Pt* system, calculated on the DCM at different $E_{c.m.}$'s for various Skyrme forces, compared with the experimental data [1]. The upper-limit of the ER cross section at $E_{c.m.} = 142.5$ MeV, included in Fig. 8, is not included here. The quasifission (qf) contribution in fission is also calculated, wherever required.

$E_{c.m.}$	T	$\ell_{max}(\hbar)$			ΔR (fm)			σ (mb)			
(MeV)	(MeV)	SSk	GSkI	SIII	SSk	GSkI	SIII	DCM			Expt.
								SSk	GSkI	SIII	
					Evaporation residue (ER)						
195.2	1.9944	108	110	120	2.271	2.173	1.481	259	259	260	259
183.7	1.8556	102	104	113	2.322	2.24	1.6753	253	251	257	251.4
175.2	1.7458	103	105	114	2.293	2.213	1.637	265	265	265	264.8
171	1.6889	101	103	113	2.275	2.197	1.625	218	219	218	218
167.2	1.6357	92	96	111	2.3794	2.274	1.643	235	235	234	234
165.5	1.6113	100	102	111	2.261	2.163	1.607	184	184	183	184
158.1	1.5004	89	92	108	2.288	2.175	1.498	70	70.2	70	70
154	1.4353	86	90	107	2.239	2.12	1.412	31.5	31.3	32	31.5
151	1.3856	82	86	106	2.159	2.033	1.247	5.08	5.03	4.87	5 ± 1
148.1	1.3359	77	82	105	2.089	1.96	1.093	0.7	0.7	0.67	0.7 ± 0.2
					Fission and predicted quasifission (qf)						
195.2	1.9944	108	110	120	2.996	2.989	1.94	189.4	224	224	544
					2.904	2.739	1.876	352[a]	321[a]	318[a]	
183.7	1.8556	102	104	113	2.959	2.871	1.94	177.6	200	230	371
					2.875	2.704	1.83	194[a]	171[a]	140[a]	
175.2	1.7458	103	105	114	2.937	2.825	1.8945	208	212	230	232.9
					2.682	2.515		25.2[a]	21.2[a]		
171	1.6889	101	103	113	2.8403	2.685	1.793	142.8	141.2	139.4	138
165.5	1.6113	100	102	111	2.701	2.539	1.649	31	31.4	31.4	31.2

[a]Symbolizes quasifission (qf) contribution.

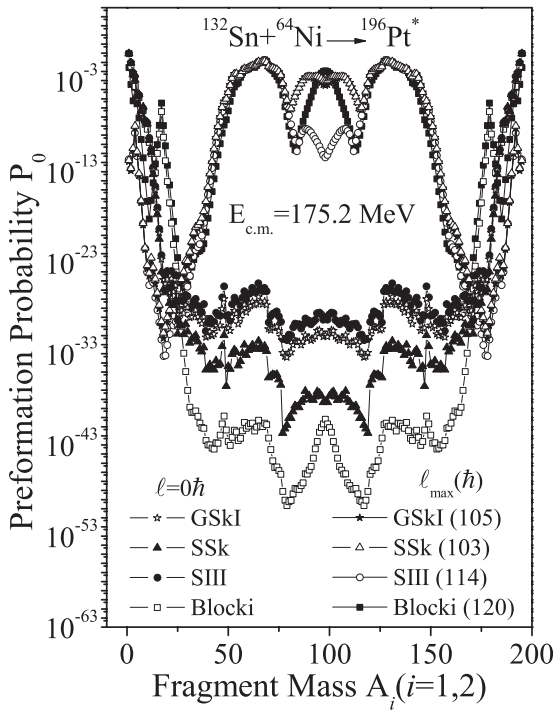

FIG. 2. Preformation probability P_0 as a function of fragment mass A_i corresponding to the fragmentation potential in Fig. 1(a).

fragments. The same is true for SIII (solid line with hollow circle) and the potential of Blocki *et al*. (solid line with rectangle), except that the latter one also favors a contribution from the symmetric mass distribution (the minimum at $A/2$ is relatively deeper). The contribution of asymmetric fragments for the SIII force is similar to other two Skyrme forces (GSkI and SSk), the difference being only in the magnitude. In other words, for all four cases the potential energy minima are stronger at the asymmetric fragments than the symmetric fragments. One may also notice that at $\ell = 0$, for all four interactions, the contribution of the ER is more prominent than the symmetric or asymmetric fission fragments, whereas at $\ell = \ell_{max}$ the fission fragments start competing with the ER, the lighter fragments.

We have also tested the role of changing the radioactive ^{132}Sn beam to a stable ^{112}Sn beam by calculating the fragmentation potential for ^{176}Pt*, using all the three Skyrme forces and the potential of Blocki *et al*., as shown in Fig. 1(b). The interesting result is that there is a noticeable change in the structure of $V(A_2)$ by adding or subtracting 20 neutrons; i.e., the predominantly asymmetric fission distribution for ^{196}Pt* changes to a predominantly symmetric one for ^{176}Pt*, independent of the choice of nuclear interaction potential. Such a change in fission mass distribution provides the possibility of studying the fine- or sub-structure in fission products of Pt* isotopes.

The above results from fragmentation potentials can be better understood in terms of the preformation factor P_0, plotted in Fig. 2 as a function of A_i. We notice from Fig. 2 that, in the decay of ^{196}Pt* at $\ell = \ell_{max}$, the contribution of the asymmetric fragment (AF) component is predominant for all four interactions considered. The preformation factors for GSkI (solid line with star) and SSk (solid line with hollow triangle) forces are overlapping with each other, indicating the preformation of the same (asymmetric and symmetric) fragments for the two forces. Interestingly, for all the interactions, the AF component is nearly the same. The calculations are made within the fitting of one parameter, the "neck length" parameter ΔR, for each chosen force, given in Table I and Fig. 3 for all the three processes of ER, fission, and qf.

Figure 4 shows the comparison of experimental data [1] on σ_{ER} and σ_{fiss} with DCM-based calculations for the three Skyrme forces (a) GSkI, (b) SSk, and (c) SIII, for the neck length parameter ΔR obtained in each case as plotted in Fig. 3. Apparently the fits obtained are good for σ_{ER}, but the fission

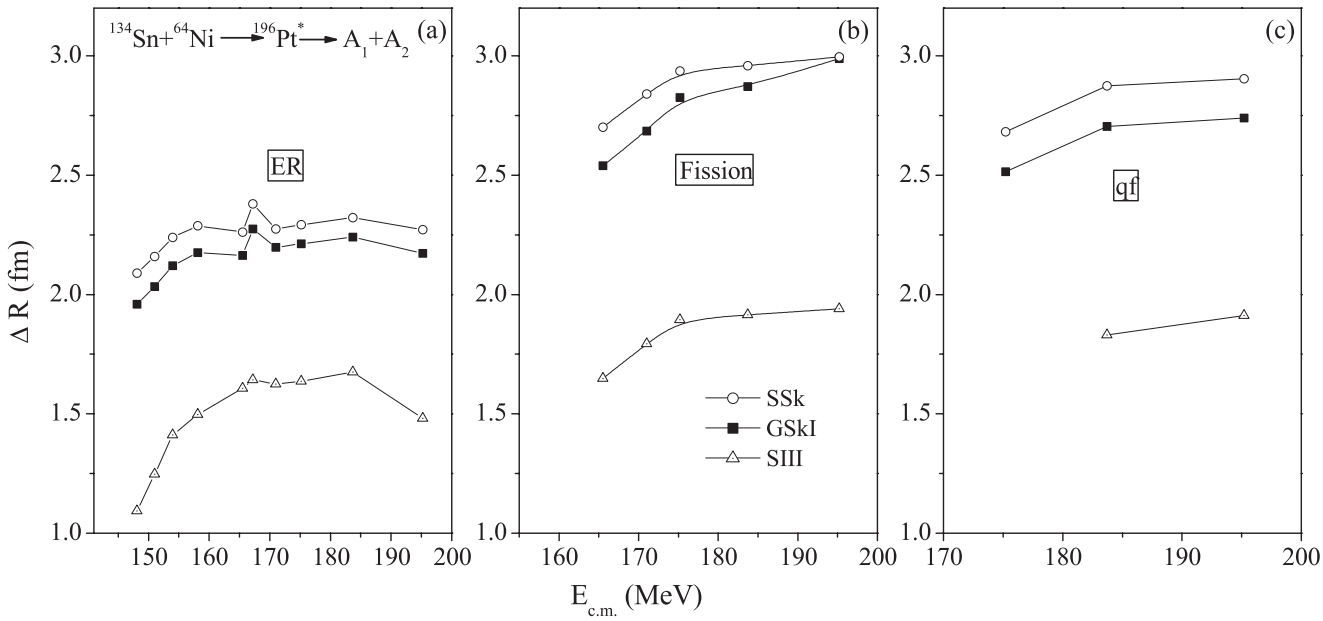

FIG. 3. The neck-length parameter ΔR plotted as a function of $E_{c.m.}$ for (a) ER, (b) fission, and (c) qf processes, using the Skyrme forces SSk (solid line with hollow circle), GSkI (solid line with rectangle) and SIII (solid line with hollow triangle).

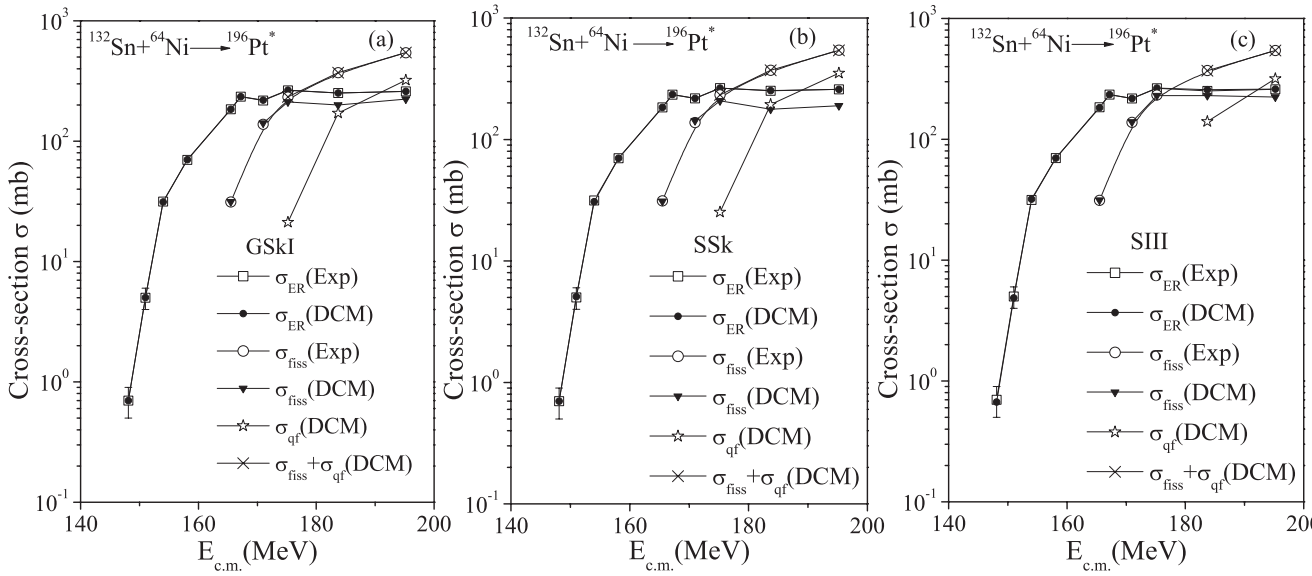

FIG. 4. Comparison of experimental evaporation residue σ_{ER} and fission cross section σ_{fiss} for the ^{132}Sn + ^{64}Ni reaction [1], with calculations made in the DCM, using the three Skyrme forces (a) GSkI, (b) SSk, and (c) SIII.

data at the highest two or three center-of-mass energies $E_{c.m.}$ did not fit for either of the Skyrme forces. At these higher $E_{c.m.}$ values, the qf process seems to compete with the fission, and the sum of these two, i.e., $\sigma_{fiss} + \sigma_{qf}$, fits the available data nicely. We notice that, for GSkI and SSk forces, qf content appears at the highest three $E_{c.m.}$ values, whereas, similar to the potential of Blocki *et al.* [5], for the SIII force it comes into the picture only at the two highest energies. In other words, for each Skyrme force, the DCM stresses the presence of noncompound qf content in fission cross sections at above-barrier energies.

Figure 5 shows the variation of the barrier lowering parameter ΔV_B as a function of $E_{c.m.}$ for the three chosen Skyrme forces, in the case of $\ell = \ell_{max}$ for the mass-1 particle.

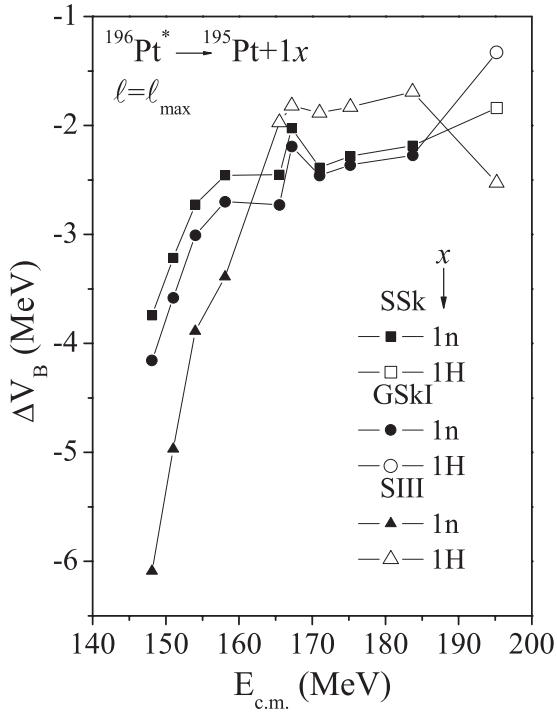

FIG. 5. Barrier-lowering parameter ΔV_B as a function of $E_{c.m.}$ for the mass-1 particle at $\ell = \ell_{max}$ for SSk, GSkI, and SIII Skyrme forces.

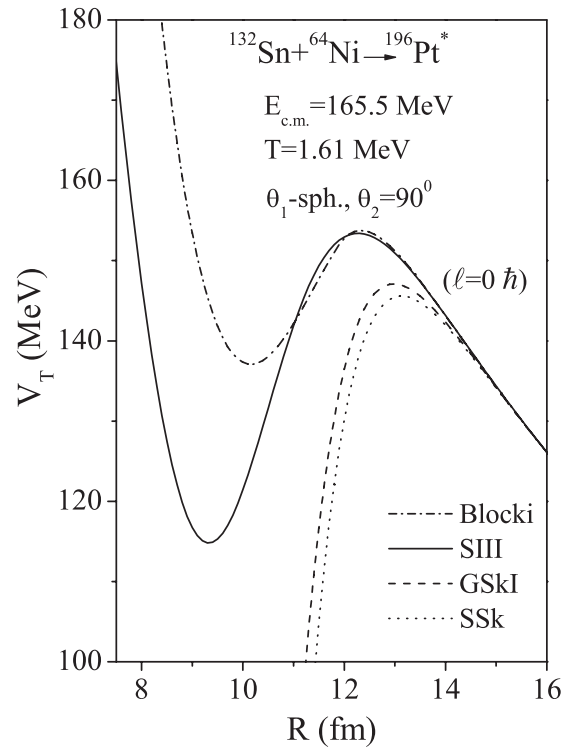

FIG. 6. Interaction potentials $V(R)$ of ^{132}Sn + ^{64}Ni for the three Skyrme forces and the potential of Blocki *et al.* at fixed $E_{c.m.}$ and θ_i values for coplanar nuclei ($\Phi = 0^0$).

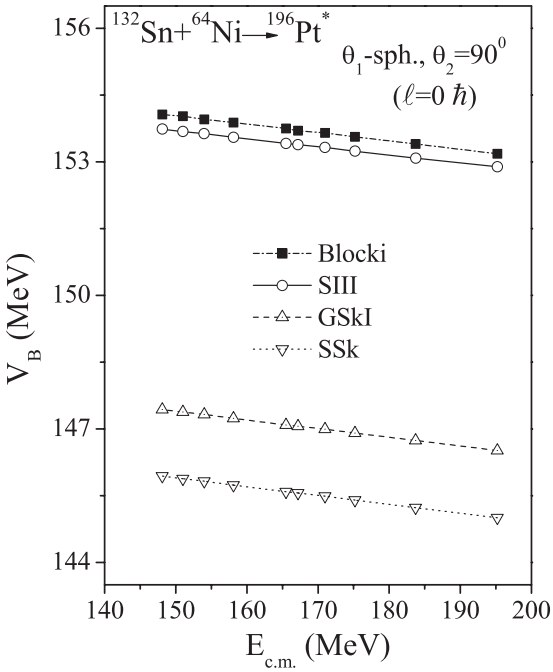

FIG. 7. Barrier height V_B as a function of $E_{\text{c.m.}}$ for ^{132}Sn + ^{64}Ni, using the three Skyrme forces SIII (solid line), GSkI (dashed line) and SSk (dotted line), and the potential of Blocki *et al*. (dashed-dot line) at fixed θ_i values for coplanar nuclei ($\Phi = 0^0$).

We notice that ΔV_B increases (i.e., becomes more negative) for below-barrier energies, and its contribution increases for the force with a higher barrier. Figure 6 shows that the barrier is highest for the SIII force (solid line), and hence in Fig. 5 the barrier lowering ΔV_B at sub-barrier energies is largest for the SIII force. In fact, ΔV_B is another representation of the neck-length parameter ΔR. It may be relevant to note that the hump in the values of ΔR for ER at $E_{\text{c.m.}} = 167.2$ MeV in both Figs. 3(a) and 5 represents the absence of data points for fission at this energy.

B. Fusion cross sections for ^{196}Pt* using the ℓ-summed extended-Wong model

The fusion cross section is the sum of the ER and fission cross sections, to which the extended-Wong model is applicable for a best fit to determine the $\ell_{\max}$ value. The barrier characteristics (V_B^ℓ, R_B^ℓ, and $\hbar\omega_\ell$), which are extracted from the scattering potentials at all the angles (coplaner in present study) and ℓ values up to $\ell_{\max}$, are the main inputs in the Wong model. Figure 6 shows the total interaction potential for ^{132}Sn + ^{64}Ni → ^{196}Pt* at fixed $E_{\text{c.m.}}$ and θ_i's for the $\ell = 0$ case. Figure 7 shows the variation of barrier height V_B with $E_{\text{c.m.}}$ for the $\ell = 0$ case of the same reaction, using all the potentials calculated in Fig. 6. It is clear from Figs. 6 and 7 that the barrier characteristics of the SIII parametrization and that of Blocki *et al*. are similar, and hence the results associated with these interactions are also close to each other. Similarly, the barrier characteristics of GSkI and SSk parametrizations are also close to each other, and hence so also are their results.

Figure 8(a) shows the fusion excitation function, i.e., the calculated fusion cross section as a function of center-of-mass energy $E_{\text{c.m.}}$ for the ^{132}Sn + ^{64}Ni reaction using the three illustrated Skyrme forces in the extended-Wong model, compared with the experimental data [1]. Apparently, the extended-Wong model calculations for GSkI and SSk forces fit the data nicely at both above- and below-barrier energies, but the SIII force does not fit the data for below-barrier energies, and hence needs barrier modifications to be included in order to fit the data. The corresponding deduced $\ell_{\max}$ values, for the best possible fits of fusion cross sections with the three Skyrme forces used in Fig. 8(a), are presented in Fig. 8(b). Notice that

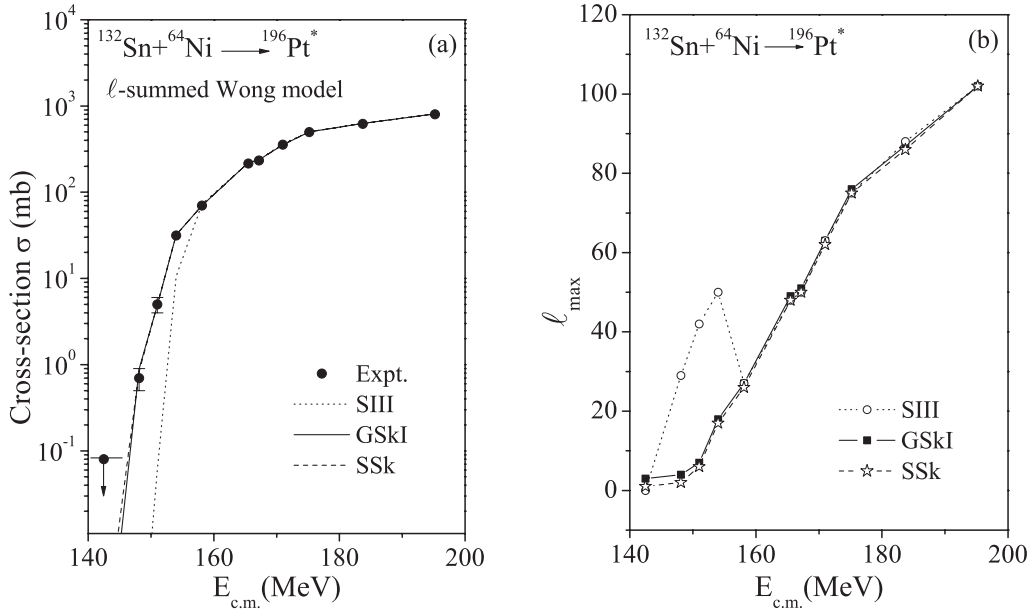

FIG. 8. (a) Fusion excitation functions of ^{132}Sn + ^{64}Ni → ^{196}Pt* using the extended-Wong model, and (b) deduced $\ell_{\max}$ values vs. $E_{\text{c.m.}}$, using the Skyrme forces SIII (dotted line), GSkI (solid line), and SSk (dashed line).

ℓ_{max} as a function of $E_{c.m.}$ varies smoothly for best-fit GSkI and SSk forces, but for the SIII force where the fit is not so good at sub-barrier energies, $\ell_{max}(E_{c.m.})$ varies erratically, which could certainly be smoothed by adding appropriate barrier lowering or barrier narrowing empirically. This kind of empirical barrier modification was attempted in one of our earlier works (see Ref. [9] for details).

It may be noted that the significant difference between the predications of the older (SIII) and the modern forces (GSkI and SSk) arises due to the different barrier characteristics. As shown in Fig. 7, the $E_{c.m.}$ dependence of the barrier height V_B for recent forces is $\sim$7 MeV lower compared to the older SIII force or the force of Blocki *et al*. Similar behavior is presented by the other two barrier properties (R_B and $\hbar\omega$) of these forces (not shown here). Since these barrier properties are the main ingredient of the Wong model, the comparison in the data is better for the new Skyrme forces with lower barriers.

IV. SUMMARY

We have studied the decay of CN ^{196}Pt*, formed in the ^{132}Sn + ^{64}Ni reaction, within the framework of the DCM, including the effects of deformation and orientation degrees of freedom. The fusion cross sections are also calculated independently by using the ℓ-summed extended-Wong Model. Both the model calculations use the nuclear proximity potential derived from the SEDF-based semiclassical ETF method with densities added under the frozen-density approximation.

Within the DCM, it is found that for the chosen three Skyrme forces GSkI, SSk, and SIII, the decay process presents the same pattern for the fragmentation potential as well as the preformation probability, indicating that asymmetric fission contributes more than symmetric fission. For all the Skyrme forces, the ER process contributes more at lower ℓ values, whereas the fission fragments start competing with ER as the ℓ value increases. However, the predominantly asymmetric pattern changes to an symmetric one with a decrease of the N/Z ratio of the CN, leading to the possibility of addressing the isospin effects in Pt* nuclei. The reversal of behavior of fission fragments, i.e., from asymmetric to symmetric, with a decrease in the N/Z ratio holds true for a variety of nuclear interaction potentials used to study the reaction dynamics of Pt isotopes. Another interesting result is that barrier lowering is required for ER cross sections at sub-barrier energies, and the fission cross sections show the necessity of qf contribution at the highest two or three energies, depending on the Skyrme force used.

The ℓ-summed extended-Wong model fits the total fusion cross section (sum of ER and fission cross sections) for the Skyrme forces GSkI and SSk, with proper dependence of deduced ℓ_{max} on $E_{c.m.}$, not requiring any additional barrier lowering or barrier narrowing for a best fit to data. However, the force SIII demands barrier modification, as the corresponding deduced ℓ_{max} in this case varies erratically or unphysically with $E_{c.m.}$. Interestingly, the ℓ-summed extended-Wong model fits the high-energy fusion cross section data nicely, without any explicit knowledge of the qf component, whereas the same can be worked out exactly in the framework of the DCM. Note that qf component could not be separated out experimentally in this reaction, and the prediction of qf at the highest two or three energies calls for a further experimental verification.

Concluding, as the reaction under study involves the neutron-rich radioactive ^{132}Sn beam, the old Skyrme force SIII and the potential of Blocki *et al*. require barrier modification, because in the fitting of parameters of the SIII force the isospin effect was not taken into account, and becuase the potential of Blocki *et al*. is less sensitive toward the isospin. However, the Skyrme forces GSkI and SSk are improved with respect to the recent experimental data, and the parameters of these forces are determined by fitting several properties of some normal and isospin-rich nuclei. Therefore, the GSkI and SSk forces are expected to perform better for isospin-rich colliding nuclei, such as the one under investigation. In other words, the dynamics of a system can be explained by using the appropriate Skyrme force whose parameters are fitted for the region to which it belongs.

ACKNOWLEDGMENTS

Financial support from the Council of Scientific and Industrial Research (CSIR) and the Department of Science and Technology (DST), New Delhi, is gratefully acknowledged.

[1] J. F. Liang *et al*., Phys. Rev. C **75**, 054607 (2007); J. F. Liang, D. Shapira, C. J. Gross, R. L. Varner, J. R. Beene, P. E. Mueller, and D. W. Stracener, *ibid*. **78**, 047601 (2008).
[2] C. L. Jiang *et al*., Phys. Rev. C **71**, 044613 (2005); Phys. Rev. Lett. **93**, 012701 (2004).
[3] S. Misicu and H. Esbensen, Phys. Rev. Lett. **96**, 112701 (2006); Phys. Rev. C **75**, 034606 (2007).
[4] R. K. Gupta, in *Clusters in Nuclei*, Lecture Notes in Physics 818, Vol. I, edited by C. Beck (Springer-Verlag, Berlin, 2010), p. 223.
[5] M. K. Sharma, S. Kanwar, G. Sawhney, R. K. Gupta, and W. Greiner, J. Phys. G: Nucl. Part. Phys. **38**, 055104 (2011).
[6] S. K. Arun, R. Kumar, and R. K. Gupta, J. Phys. G: Nucl. Part. Phys. **36**, 085105 (2009).
[7] R. K. Gupta, S. K. Arun, R. Kumar, and M. Bansal, Nucl. Phys. A **834**, 176c (2010).
[8] R. K. Gupta and M. Bansal, Int. Rev. Phys. (I.RE.PHY.) **5**, 74 (2011).
[9] R. Kumar, M. Bansal, S. K. Arun, and R. K. Gupta, Phys. Rev. C **80**, 034618 (2009).
[10] R. Kumar, M. K. Sharma, and R. K. Gupta, Nucl. Phys. A **870-871**, 42 (2011); R. Kumar and R. K. Gupta, J. Phys.: Conf. Ser. **312**, 082025 (2011).
[11] J. Blocki, J. Randrup, W. J. Swiatecki, and C. F. Tsang, Ann. Phys. (NY) **105**, 427 (1977).
[12] R. K. Gupta, D. Singh, R. Kumar, and W. Greiner, J. Phys. G: Nucl. Part. Phys. **36**, 075104 (2009).
[13] B. Grammoticos and A. Voros, Ann. Phys. **123**, 359 (1979); **129**, 153 (1980).
[14] M. Brack, C. Guet, and H.-B. Hakansson, Phys. Rep. **123**, 275 (1985).
[15] J. Bartel and K. Bencheikh, Eur. Phys. J. A **14**, 179 (2002).

[16] G.-Q. Li, J. Phys. G: Nucl. Part. Phys. **17**, 1 (1991).
[17] C. Y. Wong, Phys. Rev. Lett. **31**, 766 (1973).
[18] R. Kumar, Phys. Rev. C **84**, 044613 (2011).
[19] R. K. Gupta, M. Balasubramaniam, R. Kumar, N. Singh, M. Manhas, and W. Greiner, J. Phys. G: Nucl. Part. Phys. **31**, 631 (2005).
[20] B. K. Agrawal, S. K. Dhiman, and R. Kumar, Phys. Rev. C **73**, 034319 (2006).
[21] J. Friedrich and P.-G. Reinhard, Phys. Rev. C **33**, 335 (1986).
[22] R. K. Gupta, D. Singh, and W. Greiner, Phys. Rev. C **75**, 024603 (2007).
[23] P. Chattopadhyay and R. K. Gupta, Phys. Rev. C **30**, 1191 (1984).
[24] L. R. B. Elton, *Nuclear Sizes* (Oxford University Press, London, 1961).
[25] H. de Vries, C. W. de Jager, and C. de Vries, At. Data Nucl. Data Tables **36**, 495 (1987).
[26] R. K. Gupta, N. Singh, and M. Manhas, Phys. Rev. C **70**, 034608 (2004).
[27] S. Shlomo and J. B. Natowitz, Phys. Rev. C **44**, 2878 (1991).
[28] G. Royer and J. Mignen, J. Phys. G: Nucl. Part. Phys. **18**, 1781 (1992).
[29] P. Möller, J. R. Nix, W. D. Myers, and W. J. Swiatecki, At. Data Nucl. Data Tables **59**, 185 (1995).
[30] N. J. Davidson, S. S. Hsiao, J. Markram, H. G. Miller, and Y. Tsang, Nucl. Phys. A **570**, 61c (1994).
[31] W. Myers and W. J. Swiatecki, Nucl. Phys. A **81**, 1 (1966).
[32] S. Kumar and R. K. Gupta, Phys. Rev. C **55**, 218 (1997).
[33] H. S. Khosla, S. K. Malik, and R. K. Gupta, Nucl. Phys. A **513**, 115 (1990).
[34] D. L. Hill and J. A. Wheeler, Phys. Rev. **89**, 1102 (1953); T. D. Thomas, *ibid.* **116**, 703 (1959).